Breaking Rayleigh's Law with Spatially Correlated Disorder to Control Phonon Transport

Simon Thébaud, L. Lindsay, T. Berlijn

Breaking Rayleigh's law with spatially correlated disorder to control phonon transport

S. Thébaud,[1,2,*] L. Lindsay,[1] and T. Berlijn[3,4,†]

[1] *Materials Science and Technology Division, Oak Ridge National Laboratory, Oak Ridge, Tennessee 37831, USA*
[2] *INSA Rennes, Institut Foton, UMR 6082, 35700 Rennes, France*
[3] *Center for Nanophase Materials Sciences, Oak Ridge National Laboratory, Oak Ridge, Tennessee 37831, USA*
[4] *Computational Sciences and Engineering Division, Oak Ridge National Laboratory, Oak Ridge, Tennessee 37831, USA*

Controlling thermal transport in insulators and semiconductors is crucial for many technological fields such as thermoelectrics and thermal insulation, for which a low thermal conductivity (κ) is desirable. A major obstacle for realizing low κ materials is Rayleigh's law, which implies that acoustic phonons, which carry most of the heat, are insensitive to scattering by point defects at low energy. We demonstrate, with large scale simulations on tens of millions of atoms, that isotropic long-range spatial correlations in the defect distribution can dramatically reduce phonon lifetimes of important low-frequency heat-carrying modes, leading to a large reduction of κ – potentially an order of magnitude at room temperature. We propose a general and quantitative framework for controlling thermal transport in complex functional materials through structural spatial correlations, and we establish the optimal functional form of spatial correlations that minimize κ. We end by briefly discussing experimental realizations of various correlated structures.

Introduction. Thermal transport properties of solids are crucially important to a range of technologies. For some applications, such as electronics or fusion reactors, high thermal conductivities are desirable to evacuate heat from its source [1–3]. For others, like thermal barriers and thermoelectric modules, high thermal resistivity is critical [4, 5]. In the latter cases, relevant materials are generally electronic insulators and semiconductors and thermal transport is dominated by lattice vibrations (phonons). Defects and disorder are often engineered in such materials to scatter heat-carrying phonons and reduce the lattice thermal conductivity [6–8].

However, a major impediment to achieving ultralow conductivities is Rayleigh's law which, in this context, states that phonons are scattered by point defects at a rate proportional to the fourth power of their frequency: $1/\tau \propto \omega^4$ [9]. This law is most famous in the context of light propagation, as it is responsible for the blue color of the sky. In solids, it is widely held to hold true for low frequency phonons scattering from atomic-scale defects such as vacancies or substitutional atoms. Because ω^4 decreases rapidly with ω, Rayleigh's law implies that such disorder is inefficient at scattering acoustic phonons – which typically carry most of the heat – at low energy (see Fig. 1) [10]. Consequently, researchers have sought to lower the lifetimes of these long-wavelength phonons by introducing disordered nanostructures of various size such as granular structures, dislocations, or nanoparticles [11–15]. Based largely on the rule of thumb that phonons are most efficiently scattered by defects of size comparable to their wavelength, attempts have been made at combining these different types of disorder to target acoustic phonons over multiple frequency ranges, with various degrees of success. Thus far, experimental efforts have received little theoretical guidance, instead relying on empirical models and trial and error synthesis and characterization [16–18].

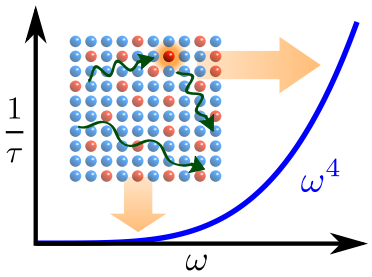

Figure 1. The ω^4 Rayleigh's law for phonon-disorder inverse lifetimes. Inset: low-ω phonons are insensitive to randomly distributed point defects, contrary to high-ω phonons.

As is well-known in optics, spatially correlated media can be used to manipulate wave scattering and propagation [19, 20]. In the context of electron and phonon transport, some perturbative field theoretical calculations have been carried out for short-range and power-law decaying correlations in the 1980's, but the main focus was on Anderson localization properties, not on the reduction of electrical or thermal conductivities [21, 22]. More recently, work has been devoted to studying phonon transport in one-dimensional chains with various forms of correlated disorder [23–26]. However, this field also has a strong fundamental focus since one-dimensional or quasi-one-dimensional systems are difficult to synthesize, let alone scale up industrially. Most technological applications require three-dimensional bulk compounds that typically display relatively isotropic properties. In particular, the formalism of spatial correlations has not been brought to bear on the long-standing effort to impede heat conduction in bulk semiconductors and insulators.

In this work, we show that Rayleigh's law can be

* E-mail: simon.thebaud@insa-rennes.fr
† E-mail: berlijnt@ornl.gov

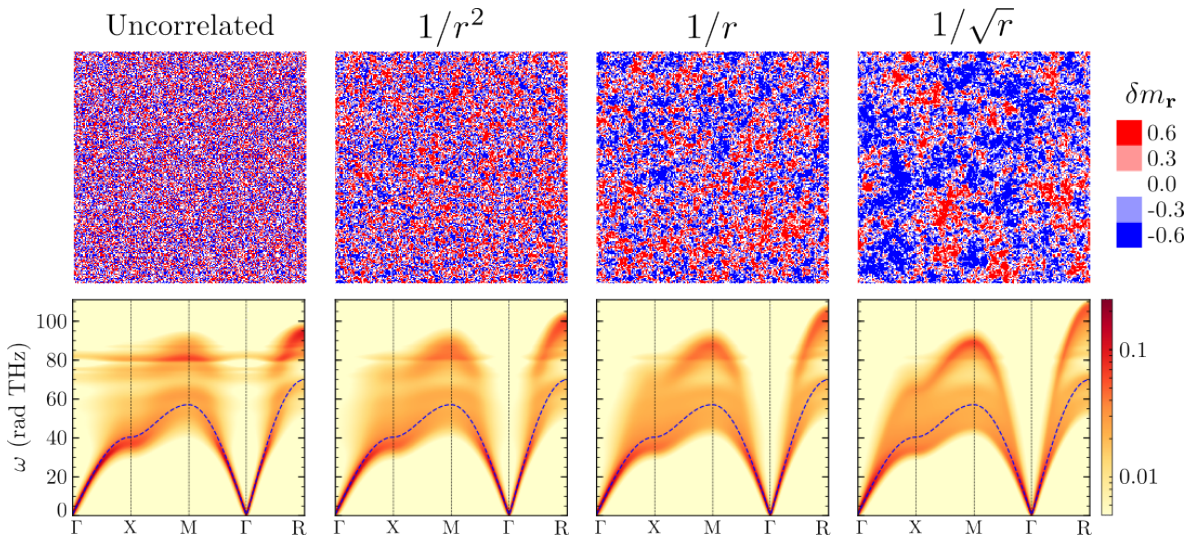

Figure 2. Top: 2D cuts of the mass distribution in supercells of size $200 \times 200 \times 200$ atoms (each pixel representing an atom) with several power-law decaying correlations $C(\boldsymbol{r}) \propto 1/r^{\alpha}$ with $\alpha = \infty$ (uncorrelated) and $\alpha = 2$, 1, and 0.5. The color scale denotes the discrete relative difference from the average mass, with five atomic species present in the supercell. Bottom: the phonon spectral function $A(\boldsymbol{k}, \omega)$ calculated by the CPGF method, together with the VCA dispersion (dashed blue line).

broken at all frequencies by atomic mass point defects with isotropic long-range spatial correlations, potentially yielding a suppression of κ by an order of magnitude at room temperature. We obtain these results by perturbative calculations and non-perturbative Green's function techniques on model spring-mass systems featuring tens of millions of atoms. Furthermore, we analytically determine the optimal correlations that minimize κ, and evaluate the impact of finite correlation lengths. Our quantitative theory can be generalized to force-constant disorder, providing a unifying framework to describe phonon-disorder scattering in materials featuring nanostructures and complex nanoscale geometries. As such, it will allow theory to guide experiments towards a more refined control of lattice thermal transport.

Formalism. Going beyond the rule of thumb relating defect size with phonon wavelength, we will explain more precisely how spatial correlations affect phonon scattering. For simplicity, we consider in this work a generic spring-mass model of mass-disordered alloy on a simple cubic lattice with five different atomic masses in roughly equal proportions and other physical parameters comparable to SiGe alloys (see the supplementary material [27] for details). The presence of mass disorder couples two phonon modes of wavevectors $\boldsymbol{k}$ and $\boldsymbol{k}+\boldsymbol{q}$ with a coupling matrix element $g_{\boldsymbol{q}}$, allowing mode $\boldsymbol{k}$ to scatter into mode $\boldsymbol{k}+\boldsymbol{q}$. In second-order perturbation theory, the phonon-disorder transport scattering rate for mode $\boldsymbol{k}$ is given by $1/\tau_{\boldsymbol{k}}^{\mathrm{d,tr}} = \frac{\pi}{\omega_{\boldsymbol{k}}} \sum_{\boldsymbol{q}} \left\langle |g_{\boldsymbol{q}}|^2 \right\rangle (1 - \cos(\theta_{\boldsymbol{k}+\boldsymbol{q},\boldsymbol{k}})) \delta(\omega_{\boldsymbol{k}+\boldsymbol{q}}^2 - \omega_{\boldsymbol{k}}^2)$ where $\theta_{\boldsymbol{k}+\boldsymbol{q},\boldsymbol{k}}$ is the angle between the velocities of modes $\boldsymbol{k}$ and $\boldsymbol{k}+\boldsymbol{q}$. The factor $1-\cos(\theta_{\boldsymbol{k}+\boldsymbol{q},\boldsymbol{k}})$, often neglected, accounts for the fact that forward scatterings contribute less to thermal resistivity than backward scattering, and must be included here for reasons that are to become clear. In this expression, only the disorder-average of $|g_{\boldsymbol{q}}|^2$ matters:

$$\left\langle |g_{\boldsymbol{q}}|^2 \right\rangle = \omega^4 \frac{1}{N} \sum_{\boldsymbol{r}} C(\boldsymbol{r}) e^{-i\boldsymbol{q}\cdot\boldsymbol{r}} \tag{1}$$

The right-hand side features the spatial Fourier transform (FT) of the mass correlation function $C(\boldsymbol{r}) = \langle \delta m_{\boldsymbol{r}}\, \delta m_{\boldsymbol{0}} \rangle$, where $\delta m_{\boldsymbol{r}}$ is the relative mass perturbation at site $\boldsymbol{r}$. In the absence of correlations, $C(\boldsymbol{r}) = \langle \delta m^2 \rangle \delta_{\boldsymbol{r0}}$ and only the ω^4 factor remains, leading to Rayleigh scattering and to weak scattering of heat-carrying low-frequency acoustic modes. However, it is possible to manipulate and redistribute the matrix elements within the first Brillouin zone by introducing correlations, i.e., going beyond randomly distributed defects. In particular, irrespective of the short-range behavior, the FT of a long-range power-law decaying correlation function $C(\boldsymbol{r}) \propto 1/r^{\alpha}$ behaves in three dimensions as $1/q^{3-\alpha}$, concentrating the matrix elements close to the Brillouin zone center if $\alpha < 3$. Thus, low-energy phonons are scattered more effectively at the price of increased forward scattering for the high-energy phonons. In this case, second-order perturbative calculations of the low-frequency phonon-disorder transport scattering rates suggest that they should decrease as $\omega^{1+\alpha}$ instead of ω^4 [27], consistent with previous perturbative calculations [21, 22]. This modified power law implies much more efficient scattering of the heat-carrying acoustic phonons than from Rayleigh scattering, leading to reduced thermal conductivity.

To test this idea, we built large disordered supercells spanning tens of millions of lattice sites in which we introduced mass disorder characterized by power-law decaying correlation functions. We also considered uncorrelated

mass disorder as a reference. From the real-space dynamical matrix of these supercells, we used the Chebyshev polynomials Green's function method (CPGF) to obtain the phonon Green's function by a numerical expansion on the basis of Chebyshev polynomials [10, 28–31]. This approach is nonperturbative, allowing a full treatment of disorder effects. From the Green's function, we calculated the phonon spectral function, the phonon lifetimes, and the frequency-dependent thermal conductivity. We also obtained κ from the Boltzmann transport equation (BTE) under the relaxation time approximation using transport scattering rates calculated from Fermi's golden rule (FGR). More details on the methodology, formalism and computational limitations can be found below and in [27]. Of note, we use the term 'inverse lifetime' here rather than 'scattering rate' for phonon-disorder spectral linewidths to emphasize the distinction with 'transport scattering rate' that includes a vertex correction factor.

Results and discussion. The top panel of Fig. 2 shows two-dimensional cuts of the mass distribution in supercells with 200^3 atoms characterized by a correlation function $C(\boldsymbol{r}) \propto 1/r^\alpha$ with $\alpha = \infty$ (uncorrelated) and $\alpha = 2$, 1, and 0.5. The mass distributions, involving five atomic species, are implemented 'by hand' to give the desired correlations (see [27] for details). The mass distribution in the uncorrelated case is simply white noise, but as more and more long-range correlations are introduced, clusters and nanostructures of heavy and light atoms appear and grow larger, keeping however a broad size distribution. The bottom panel of Fig. 2 shows the corresponding CPGF-calculated phonon spectral function $A(\boldsymbol{k}, \omega)$ on a high-symmetry path in the first Brillouin zone. For a given plane-wave mode of wavevector $\boldsymbol{k}$, $A(\boldsymbol{k}, \omega)$ represents the energy distribution of that mode, and is close to the dynamical structure factor probed by inelastic X-ray and neutron scattering [32, 33]. In the absence of disorder, plane waves are normal modes of the system so $A(\boldsymbol{k}, \omega) = \delta(\omega - \omega_{\boldsymbol{k}})$. In the presence of disorder, the spectral peak is shifted (phonon frequencies are renormalized) and broadened (phonons acquire a finite lifetime). For visualization purposes, an artificial Lorentzian broadening of 1 rad THz is added to the physical broadening from mass disorder in Fig. 2. In all cases, low-frequency acoustic phonons are well defined in the sense that their broadening is much smaller than their central frequency, and they match the dispersion given by the virtual crystal approximation (VCA), which simply averages the atomic masses [34] and for our single-site model results in three degenerate acoustic phonon branches. The uncorrelated spectrum (leftmost panel) features ill-defined phonons above 40 rad THz whose broadening is comparable to their frequency (diffusons in Allen and Feldman's terminology [35]), and some flat branches above the VCA spectrum arising from isolated light atoms. The most obvious effect of long-range correlations is to introduce more structure to the flat branches above the VCA. This indicates that, for $1/\sqrt{r}$ correlations, the phonons almost start to propagate inside the domains as if they were infinite, leading to emergent light and heavy dispersions [31, 36]. Nevertheless, correlations do not seem to drastically alter the lifetimes of high-frequency VCA modes.

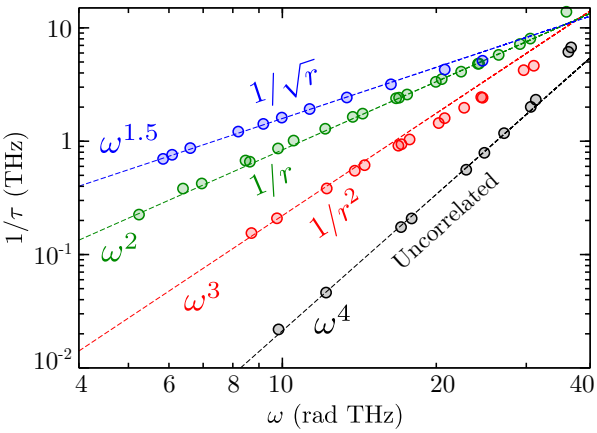

Figure 3. Phonon-disorder inverse lifetimes extracted from the width of the CPGF-calculated spectral peaks for several power-law decaying correlations.

For phonon modes below 40 rad THz whose full width at half maximum (FWHM) can be defined, we extracted the FWHM that corresponds to the disorder-limited inverse lifetime of the mode, shown in Fig. 3 (the spectral functions of selected modes in the relevant frequency range are shown in [27]). In the uncorrelated case, we find the usual ω^4 low-frequency behavior. However, we find an ω^3 law for $1/r^2$ correlations, an ω^2 law for $1/r$ correlations and an $\omega^{1.5}$ law for $1/\sqrt{r}$ correlations, with lifetimes orders of magnitude smaller than in the uncorrelated case. This validates the perturbative result that $1/r^\alpha$ correlations lead to a $\omega^{1+\alpha}$ power law, and confirms that it is possible to circumvent Rayleigh scattering by introducing long-range spatial correlations.

From Fig. 3, one could be tempted to conclude that the longer-range the correlations, the lower the thermal conductivity. As we shall see, however, this is not the case. Evaluating κ in these systems is *a priori* non-trivial, given the breakdown of the quasiparticle picture at high frequencies. To overcome this issue, we used the Green-Kubo formalism (quantum linear response theory), evaluating κ directly by the CPGF method on supercells with $1200 \times 200 \times 200$ atoms [27]. This approach, which does not rely on the phonon quasiparticle picture, includes the diffusive channel (thermal transport by broadened overlapping modes [37]) and is comparable to methods recently proposed by Isaeva [38] and Caldarelli [39] (see Ref. [10] for a discussion of the differences between these approaches). Crucially, it also takes into account all the so-called vertex corrections encoding the fact that forward scatterings contribute less to the thermal resistivity than backward scatterings [40]. Long-range correlations favor low-$\boldsymbol{q}$ matrix elements, leading to mostly forward

scattering of large-wavevector phonons. Thus, neglecting the vertex corrections would introduce large errors in the evaluation of κ. At low-frequencies, this method agrees with the thermal conductivity obtained using the standard kinetic expression (or, equivalently, solving the Boltzmann transport equation under the relaxation time approximation) with phonon-disorder transport lifetimes evaluated through second-order perturbation theory [10]. Due to the presence of the $1-\cos(\theta)$ forward scattering, the most relevant vertex corrections (ladder diagrams) are also included in this simpler approach, and we use it for the contributions to κ below 10 rad THz to avoid the prohibitive computational cost of the CPGF method at these frequencies. In all cases, we accounted for Umklapp anharmonic scattering through a simple expression $1/\tau_U = A\omega^2 T e^{-\Theta/T}$, with similar parameters as found in the literature for Si, Ge, and GaN compounds [41–46] (see also [27]). The results are shown in Fig. 4: dots correspond to the above method involving Green-Kubo CPGF calculations and the dashed lines to kinetic perturbative calculations only. Both methods are in very good agreement, indicating that the diffusive channel does not play an important role here and that the crucial physics is captured by the perturbative evaluation of the transport lifetimes. For this model, the room-temperature thermal conductivity is around $18\,\mathrm{W\,m^{-1}\,K^{-1}}$ without correlations. However, by introducing $1/r$ correlations, it is reduced to $2.5\,\mathrm{W\,m^{-1}\,K^{-1}}$, almost an order of magnitude decrease. This suggests that spatially correlated point defects can indeed be used to crush the thermal conductivity. $1/r^2$ correlations lead to a large but somewhat less effective decrease, with $4.4\,\mathrm{W\,m^{-1}\,K^{-1}}$. Perhaps more surprisingly given the results of Fig. 3, $1/\sqrt{r}$ correlations are also slightly less effective than $1/r$ correlations, with $2.9\,\mathrm{W\,m^{-1}\,K^{-1}}$. We show in [27] the same graph in log scale making the difference between the long-range correlations clearer, with a brief discussion on the importance of vertex corrections.

Why are $1/\sqrt{r}$ correlations less effective despite the shorter acoustic phonon lifetimes displayed in Fig. 3? The longer the correlation range, the more they concentrate the coupling matrix elements (1) at the center of the Brillouin Zone (at small $\boldsymbol{q}$). This leads to more foward scattering of high-frequency phonons with large wavevectors, allowing these modes to contribute more efficiently to thermal transport. Thus, to minimize the thermal conductivity, correlations should strike a balance between scatterings at all wavelengths. More precisely, for a given disorder strength $\langle \delta m^2 \rangle$, the Fourier transform $\tilde{C}(\boldsymbol{q})$ of the mass correlation function $C(\boldsymbol{r})$ must obey a constraint: $\frac{\Omega}{(2\pi)^3}\int d^3\boldsymbol{q}\,\tilde{C}(\boldsymbol{q}) = \langle \delta m^2 \rangle$, where Ω is the system size and the integral covers the Brillouin zone. If we assume that the thermal conductivity is given by the standard kinetic expression with perturbative transport phonon lifetimes (which yields excellent agreement with the full CPGF treatment, see Fig. 4), finding the optimal correlation function to minimize κ can then be recast as a classic optimization under constraint problem. We introduce a Lagrange multiplier λ and set the functional derivative of κ minus the constraint to 0:

$$\frac{\delta}{\delta\tilde{C}(\boldsymbol{q})}\left[\int \frac{d^3\boldsymbol{k}}{(2\pi)^3}\, c_v(\omega_{\boldsymbol{k}}) v_{\boldsymbol{k}}^2 \tau_{\boldsymbol{k}}^{\mathrm{tr}} - \lambda \int d^3\boldsymbol{k}\,\tilde{C}(\boldsymbol{k})\right] = 0 \quad (2)$$

where $v_{\boldsymbol{k}}$ is the velocity of mode $\boldsymbol{k}$ along the transport direction and $c_v(\omega_{\boldsymbol{k}})$ the heat capacity of that mode. $\tau_{\boldsymbol{k}}^{\mathrm{tr}} = (1/\tau_U + 1/\tau_{\boldsymbol{k}}^{\mathrm{d,tr}})^{-1}$ is the transport lifetime of mode $\boldsymbol{k}$ with $1/\tau_{\boldsymbol{k}}^{\mathrm{d,tr}} = \pi\omega_{\boldsymbol{k}}^3 \sum_{\boldsymbol{q}} \tilde{C}(\boldsymbol{q})(1-\cos(\theta_{\boldsymbol{k}+\boldsymbol{q},\boldsymbol{k}}))\delta(\omega_{\boldsymbol{k}+q}^2 - \omega_{\boldsymbol{k}}^2)$. Assuming now isotropic correlations and a Debye dispersion, eq. (2) yields the condition $1/\tau_{\boldsymbol{k}}^{\mathrm{tr}} \propto \sqrt{c_v(\omega_{\boldsymbol{k}})}\omega_{\boldsymbol{k}}^2$ (see [27] for the derivation). For high enough temperatures, c_v becomes weakly dependent on the frequency and the condition becomes that the total transport scattering is quadratic in frequency. If anharmonic scattering is also quadratic in ω, as was supposed above, then the optimal correlations are those that lead to a phonon-disorder transport scattering rate proportional to ω^2. In other words, this argument suggests that of all the possible types of isotropic correlations, $1/r$ power-law correlations are the most efficient at reducing the thermal conductivity. This is consistent with Fig. 4, although due to the simplifying assumptions in the above argument, longer-range correlations may in practice be just as efficient.

Although we have limited our investigation to the case of mass defects for simplicity, the language of spatial correlations is also applicable to force constant disorder, thus potentially encompassing all forms of static disorder. The question then arises: in which materials could favorable correlations appear or be engineered to lower κ? The Ising model is one theoretical context, widely applicable to many systems [47, 48], whose mean-field solution just so happens to yield correlations of the form $\frac{1}{r}e^{-r/\xi}$ with ξ the correlation length that diverges as T is lowered to-

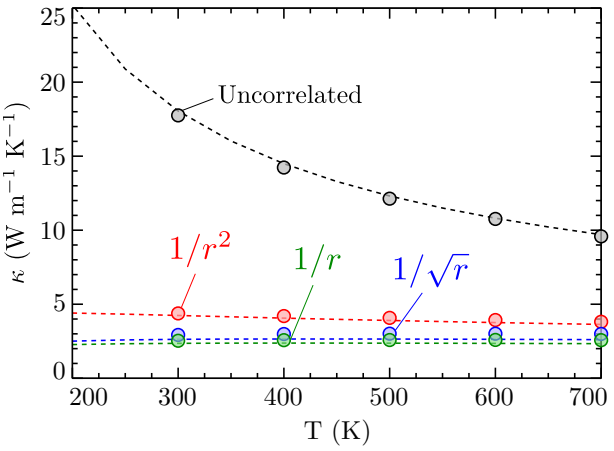

Figure 4. The thermal conductivities for several power-law decaying correlations evaluated through Green-Kubo CPGF calculations above 10 rad THz, with second-order perturbation theory below 10 rad THz (dots) and through perturbation theory only (dashed lines).

wards the critical temperature T_c. We performed perturbative calculations showing that the presence of a correlation length is not a serious issue for reducing κ as long as it is not very small (a few Å, see [27]). Therefore, if the system was quenched from a temperature just above T_c, $1/r$ correlations would be captured and the thermal conductivity would be crushed, provided the correlations are not destroyed by phenomena such as nucleation and spinodal decomposition [15, 49, 50]. Another situation where $1/r$ correlations arise is in the strain field around dislocations, leading to a scattering rate proportional to ω due to the one-dimensional nature of the defect [51]. This linear law might be considered very efficient at scattering low-frequency phonons, but in fact the translation symmetry along the dislocation line forbids many scattering processes, which leads to a lower scattering rate. Nevertheless, the presence of a dense network of non-parallel dislocations might restore some degree of isotropy while preserving long-range strain fields, potentially yielding low thermal conductivities [52]. So-called procrystals, characterized by local orientational sum rules, are the structural or chemical equivalent of pyrochlore spin-ice materials and feature $1/r^3$ correlations [53–57]. However, the presence of topological defects, whose density might be controlled by thermal treatments, could introduce longer-range correlations. Other situations potentially involving long-range and medium-range correlations are nanoparticles and extended defects [58–60], nanodomains in relaxor ferroelectrics and charge density wave materials [61], and stacks of twisted atomic monolayers [62–65]. With this work, we provide a general, quantitative and unifying framework to understand the transport properties of disordered systems, and we open the door towards the systematic design of structure-induced transport functionalities.

Summary. Using large-scale non-perturbative numerical simulations, we showed that the ω^4 Rayleigh power law for the defect-limited inverse lifetimes of low-frequency acoustic phonons can be broken by long-range spatial correlations in the distribution of point defects. We proposed this as a strategy for tuning the lattice thermal conductivity of functional materials, and found an order of magnitude reduction of the conductivity through state-of-the art, fully quantum mechanical techniques. We showed analytically that correlations decaying as $1/r$ minimize the thermal conductivity by striking an optimal balance between scattering low-frequency and high frequency phonons. We posit that this framework can describe phonon conduction in a great variety of nanostructured systems and guide experimentalists towards a fine control of thermal transport in bulk materials.

ACKNOWLEDGEMENTS

We thank German Samolyuk for helpful discussions. This research was supported by the U.S. Department of Energy, Office of Science, Basic Energy Sciences, Materials Sciences and Engineering Division. We used resources of the Compute and Data Environment for Science (CADES) at the Oak Ridge National Laboratory, which is supported by the Office of Science of the U.S. Department of Energy under Contract No. DE-AC05-00OR22725.

[1] A. L. Moore and L. Shi, Emerging challenges and materials for thermal management of electronics, Materials Today **17**, 163 (2014).
[2] L. Hu, B. D. Wirth, and D. Maroudas, Thermal conductivity of tungsten: Effects of plasma-related structural defects from molecular-dynamics simulations, Applied Physics Letters **111**, 081902 (2017).
[3] Y. Wang and J. Zhao, Numerical simulations of thermal conductivity in void-containing tungsten: Topological feature of voids, Journal of Nuclear Materials **543**, 152601 (2021).
[4] G. J. Snyder and E. S. Toberer, Complex thermoelectric materials, Nature. Mater. **7**, 105 (2008).
[5] M. Beekman and D. G. Cahill, Inorganic Crystals with Glass-Like and Ultralow Thermal Conductivities†, Crystal Research and Technology **52**, 1700114 (2017).
[6] G. Tan, S. Hao, R. C. Hanus, X. Zhang, S. Anand, T. P. Bailey, A. J. E. Rettie, X. Su, C. Uher, V. P. Dravid, G. J. Snyder, C. Wolverton, and M. G. Kanatzidis, High Thermoelectric Performance in SnTe–AgSbTe2 Alloys from Lattice Softening, Giant Phonon–Vacancy Scattering, and Valence Band Convergence, ACS Energy Letters **3**, 705 (2018).
[7] H. Kleinke, New bulk Materials for Thermoelectric Power Generation: Clathrates and Complex Antimonides, Chemistry of Materials **22**, 604 (2010).
[8] C. J. Vineis, A. Shakouri, A. Majumdar, and M. G. Kanatzidis, Nanostructured Thermoelectrics: Big Efficiency Gains from Small Features, Adv. Mater. **22**, 3970 (2010).
[9] P. G. Klemens, The Scattering of Low-Frequency Lattice Waves by Static Imperfections, Proceedings of the Physical Society. Section A **68**, 1113 (1955).
[10] S. Thébaud, T. Berlijn, and L. Lindsay, Perturbation theory and thermal transport in mass-disordered alloys: Insights from Green's function methods, Physical Review B **105**, 134202 (2022).
[11] Z. Chen, X. Zhang, and Y. Pei, Manipulation of Phonon Transport in Thermoelectrics, Advanced Materials **30**, 1705617 (2018).
[12] B. Poudel, Q. Hao, Y. Ma, Y. Lan, A. Minnich, B. Yu, X. Yan, D. Wang, A. Muto, D. Vashaee, X. Chen, J. Liu, M. S. Dresselhaus, G. Chen, and Z. Ren, High-Thermoelectric Performance of Nanostructured Bismuth Antimony Telluride Bulk Alloys, Science **320**, 634 (2008).
[13] G. Joshi, H. Lee, Y. Lan, X. Wang, G. Zhu, D. Wang, R. W. Gould, D. C. Cuff, M. Y. Tang, M. S. Dressel-

haus, G. Chen, and Z. Ren, Enhanced Thermoelectric Figure-of-Merit in Nanostructured p-type Silicon Germanium Bulk Alloys, Nano Letters **8**, 4670 (2008).
[14] S. I. Kim, K. H. Lee, H. A. Mun, H. S. Kim, S. W. Hwang, J. W. Roh, D. J. Yang, W. H. Shin, X. S. Li, Y. H. Lee, G. J. Snyder, and S. W. Kim, Dense dislocation arrays embedded in grain boundaries for high-performance bulk thermoelectrics, Science **348**, 109 (2015).
[15] Y. Zheng, T. J. Slade, L. Hu, X. Y. Tan, Y. Luo, Z.-Z. Luo, J. Xu, Q. Yan, and M. G. Kanatzidis, Defect engineering in thermoelectric materials: What have we learned?, Chemical Society Reviews **50**, 9022 (2021).
[16] M. S. Dresselhaus, G. Chen, M. Y. Tang, R. G. Yang, H. Lee, D. Z. Wang, Z. F. Ren, J.-P. Fleurial, and P. Gogna, New Directions for Low-Dimensional Thermoelectric Materials, Adv. Mater. **19**, 1043 (2007).
[17] M. Zebarjadi, K. Esfarjani, M. S. Dresselhaus, Z. F. Ren, and G. Chen, Perspectives on thermoelectrics: From fundamentals to device applications, Energy \& Environmental Science **5**, 5147 (2012).
[18] A. J. Minnich, M. S. Dresselhaus, Z. F. Ren, and G. Chen, Bulk nanostructured thermoelectric materials: Current research and future prospects, Energy Environ. Sci. **2**, 466 (2009).
[19] K. Vynck, R. Pierrat, R. Carminati, L. S. Froufe-Pérez, F. Scheffold, R. Sapienza, S. Vignolini, and J. J. Sáenz, Light in correlated disordered media (2021).
[20] A. Dikopoltsev, H. Herzig Sheinfux, and M. Segev, Localization by virtual transitions in correlated disorder, Physical Review B **100**, 140202 (2019).
[21] S. John and M. J. Stephen, Wave propagation and localization in a long-range correlated random potential, Physical Review B **28**, 6358 (1983).
[22] Q.-J. Chu and Z.-Q. Zhang, Effect of correlations on the localization properties of electrons and phonons in the long-wavelength limit, Physical Review B **39**, 7120 (1989).
[23] I. F. Herrera-González and J. A. Méndez-Bermúdez, Controlling the size scaling of the thermal conductivity in harmonic chains with correlated mass disorder, Physics Letters A **384**, 126380 (2020).
[24] A. V. Savin, V. Zolotarevskiy, and O. V. Gendelman, Heat conduction in diatomic chains with correlated disorder, Physics Letters A **381**, 145 (2017).
[25] S. S. de Albuquerque, J. L. L. dos Santos, F. A. B. F. de Moura, and M. L. Lyra, Enhanced localization, energy anomalous diffusion and resonant mode in harmonic chains with correlated mass-spring disorder, Journal of Physics: Condensed Matter **27**, 175401 (2015).
[26] F. M. Izrailev and N. M. Makarov, Anomalous transport in low-dimensional systems with correlated disorder, Journal of Physics A: Mathematical and General **38**, 10613 (2005).
[27] More details on the model, the transport formalism and analytical calculations are provided in the Supplementary Material available online, which include Refs. [66–69].
[28] A. Ferreira and E. R. Mucciolo, Critical Delocalization of Chiral Zero Energy Modes in Graphene, Physical Review Letters **115**, 106601 (2015).
[29] A. Weiße, G. Wellein, A. Alvermann, and H. Fehske, The kernel polynomial method, Reviews of Modern Physics **78**, 275 (2006).
[30] G. Bouzerar, S. Thébaud, S. Pecorario, and C. Adessi, Drastic effects of vacancies on phonon lifetime and thermal conductivity in graphene, Journal of Physics: Condensed Matter **32**, 295702 (2020).
[31] S. Thébaud, C. A. Polanco, L. Lindsay, and T. Berlijn, Success and breakdown of the T-matrix approximation for phonon-disorder scattering, Physical Review B **102**, 094206 (2020).
[32] S. N. Taraskin and S. R. Elliott, Connection between the true vibrational density of states and that derived from inelastic neutron scattering, Physical Review B **55**, 117 (1997).
[33] H. Mutka, M. M. Koza, M. R. Johnson, Z. Hiroi, J.-I. Yamaura, and Y. Nagao, Generalized density-of-states and anharmonicity of the low-energy phonon bands from coherent inelastic neutron scattering response in the pyrochlore osmates AOs_2O_6 (A = K, Rb, Cs), Physical Review B **78**, 104307 (2008).
[34] B. Abeles, Lattice Thermal Conductivity of Disordered Semiconductor Alloys at High Temperatures, Physical Review **131**, 1906 (1963).
[35] P. B. Allen, J. L. Feldman, J. Fabian, and F. Wooten, Diffusons, locons and propagons: Character of atomie yibrations in amorphous Si, Philosophical Magazine B **79**, 1715 (1999).
[36] F. Körmann, Y. Ikeda, B. Grabowski, and M. H. F. Sluiter, Phonon broadening in high entropy alloys, npj Computational Materials **3**, 36 (2017).
[37] M. Simoncelli, N. Marzari, and F. Mauri, Unified theory of thermal transport in crystals and glasses, Nature Physics **15**, 809 (2019).
[38] L. Isaeva, G. Barbalinardo, D. Donadio, and S. Baroni, Modeling heat transport in crystals and glasses from a unified lattice-dynamical approach, Nature Communications **10**, 3853 (2019).
[39] G. Caldarelli, M. Simoncelli, N. Marzari, F. Mauri, and L. Benfatto, Many-body Green's function approach to lattice thermal transport, Physical Review B **106**, 024312 (2022).
[40] N. W. Ashcroft and N. D. Mermin, *Solid State Physics* (Saunders College, 1976).
[41] N. Mingo, Calculation of Si nanowire thermal conductivity using complete phonon dispersion relations, Physical Review B **68**, 113308 (2003).
[42] C. Jeong, S. Datta, and M. Lundstrom, Full dispersion versus Debye model evaluation of lattice thermal conductivity with a Landauer approach, Journal of Applied Physics **109**, 073718 (2011).
[43] M. Asen-Palmer, K. Bartkowski, E. Gmelin, M. Cardona, A. P. Zhernov, A. V. Inyushkin, A. Taldenkov, V. I. Ozhogin, K. M. Itoh, and E. E. Haller, Thermal conductivity of germanium crystals with different isotopic compositions, Physical Review B **56**, 9431 (1997).
[44] C. Guthy, C.-Y. Nam, and J. E. Fischer, Unusually low thermal conductivity of gallium nitride nanowires, Journal of Applied Physics **103**, 064319 (2008).
[45] T. Luo, J. Garg, J. Shiomi, K. Esfarjani, and G. Chen, Gallium arsenide thermal conductivity and optical phonon relaxation times from first-principles calculations, EPL (Europhysics Letters) **101**, 16001 (2013).
[46] J. Garg, N. Bonini, B. Kozinsky, and N. Marzari, Role of Disorder and Anharmonicity in the Thermal Conductivity of Silicon-Germanium Alloys: A First-Principles Study, Physical Review Letters **106**, 045901 (2011).
[47] S. P. Singh, *The Ising Model: Brief Introduction and Its Application* (IntechOpen, 2020).

[48] L.-L. Zhang and Y.-N. Huang, Theory of relaxor-ferroelectricity, Scientific Reports **10**, 5060 (2020).

[49] J. Androulakis, C.-H. Lin, H.-J. Kong, C. Uher, C.-I. Wu, T. Hogan, B. A. Cook, T. Caillat, K. M. Paraskevopoulos, and M. G. Kanatzidis, Spinodal Decomposition and Nucleation and Growth as a Means to Bulk Nanostructured Thermoelectrics: Enhanced Performance in Pb1-xSnxTe-PbS, Journal of the American Chemical Society **129**, 9780 (2007).

[50] S. N. Girard, K. Schmidt-Rohr, T. C. Chasapis, E. Hatzikraniotis, B. Njegic, E. M. Levin, A. Rawal, K. M. Paraskevopoulos, and M. G. Kanatzidis, Analysis of Phase Separation in High Performance PbTe–PbS Thermoelectric Materials, Advanced Functional Materials **23**, 747 (2013).

[51] R. Hanus, R. Gurunathan, L. Lindsay, M. T. Agne, J. Shi, S. Graham, and G. Jeffrey Snyder, Thermal transport in defective and disordered materials, Applied Physics Reviews **8**, 031311 (2021).

[52] R. Basu, S. Bhattacharya, R. Bhatt, M. Roy, S. Ahmad, A. Singh, M. Navaneethan, Y. Hayakawa, D. K. Aswal, and S. K. Gupta, Improved thermoelectric performance of hot pressed nanostructured n-type SiGe bulk alloys, Journal of Materials Chemistry A **2**, 6922 (2014).

[53] C. L. Henley, The "Coulomb phase" in frustrated systems, Annual Review of Condensed Matter Physics **1**, 179 (2010).

[54] A. Simonov and A. L. Goodwin, Designing disorder into crystalline materials, Nature Reviews Chemistry **4**, 657 (2020).

[55] A. R. Overy, A. B. Cairns, M. J. Cliffe, A. Simonov, M. G. Tucker, and A. L. Goodwin, Design of crystal-like aperiodic solids with selective disorder–phonon coupling, Nature Communications **7**, 10445 (2016).

[56] D. A. Keen and A. L. Goodwin, The crystallography of correlated disorder, Nature **521**, 303 (2015).

[57] D. Ormrod Morley, A. L. Goodwin, and M. Wilson, Ring structure of selected two-dimensional procrystalline lattices, Physical Review E **102**, 062308 (2020).

[58] A. Kundu, N. Mingo, D. A. Broido, and D. A. Stewart, Role of light and heavy embedded nanoparticles on the thermal conductivity of SiGe alloys, Physical Review B **84**, 125426 (2011).

[59] R. Guo and S. Lee, Mie scattering of phonons by point defects in IV-VI semiconductors PbTe and GeTe, Materials Today Physics **12**, 100177 (2020).

[60] M.-S. Jeng, R. Yang, D. Song, and G. Chen, Modeling the Thermal Conductivity and Phonon Transport in Nanoparticle Composites Using Monte Carlo Simulation, Journal of Heat Transfer **130**, 10.1115/1.2818765 (2008).

[61] R. A. Cowley, S. N. Gvasaliya, S. G. Lushnikov, B. Roessli, and G. M. Rotaru, Relaxing with relaxors: A review of relaxor ferroelectrics, Advances in Physics **60**, 229 (2011).

[62] S. E. Kim, F. Mujid, A. Rai, F. Eriksson, J. Suh, P. Poddar, A. Ray, C. Park, E. Fransson, Y. Zhong, D. A. Muller, P. Erhart, D. G. Cahill, and J. Park, Extremely anisotropic van der Waals thermal conductors, Nature **597**, 660 (2021).

[63] C. Chiritescu, D. G. Cahill, N. Nguyen, D. Johnson, A. Bodapati, P. Keblinski, and P. Zschack, Ultralow Thermal Conductivity in Disordered, Layered WSe_2 Crystals, Science **315**, 351 LP (2007).

[64] N. T. Nguyen, P. A. Berseth, Q. Lin, C. Chiritescu, D. G. Cahill, A. Mavrokefalos, L. Shi, P. Zschack, M. D. Anderson, I. M. Anderson, and D. C. Johnson, Synthesis and Properties of Turbostratically Disordered, Ultrathin WSe_2 Films, Chemistry of Materials **22**, 2750 (2010).

[65] E. C. Hadland, H. Jang, N. Wolff, R. Fischer, A. C. Lygo, G. Mitchson, D. Li, L. Kienle, D. G. Cahill, and D. C. Johnson, Ultralow thermal conductivity of turbostratically disordered $MoSe_2$ ultra-thin films and implications for heterostructures, Nanotechnology **30**, 285401 (2019).

[66] S.-i. Tamura, Isotope scattering of dispersive phonons in Ge, Physical Review B **27**, 858 (1983).

[67] S.-i. Tamura, Isotope scattering of large-wave-vector phonons in GaAs and InSb: Deformation-dipole and overlap-shell models, Physical Review B **30**, 849 (1984).

[68] G. D. Mahan, *Many Particle Physics, Third Edition* (Plenum, New York, 2000).

[69] R. J. Hardy, Energy-Flux Operator for a Lattice, Physical Review **132**, 168 (1963).

Supplementary Information: Breaking Rayleigh's law with spatially correlated disorder to control phonon transport

S. Thébaud, L. Lindsay, T. Berlijn

1 Details of the alloy model and generation of the correlated mass configurations

The model that we consider is a generic mass-disordered spring-mass system on a simple cubic lattice, with lattice constant $a = 2.47\,\text{Å}$, average atomic masses $m_0 = 50\,\text{amu}$ and nearest-neighbor interatomic force constants $2.11\,\text{eV/Å}$. These parameters lead to a maximum angular frequency $70\,\text{rad THz}$ and a sound velocity $c = 5000\,\text{m/s}$ in the virtual crystal approximation (VCA), which is comparable to SiGe alloys [1]. We assume the vibrations along x, y and z to be independent, so that only one direction is included in the calculations and a factor 3 is then added to the thermal conductivities.

The anharmonicity is taken into account through a frequency-dependent phonon-phonon Umklapp scattering rate

$$\frac{1}{\tau^{\text{U}}(\omega)} = A\omega^2 T e^{-\Theta/T} \tag{1}$$

with $A = 3{\times}10^{-7}\,\text{ps/K}$ and $\Theta = 140\,\text{K}$. These parameters are again similar to those evaluated in the literature from fitting thermal conductivity measurements of Si and Ge crystals [2, 1, 3], but also certain III-V semiconductors such as GaN [4]. In addition, they yield Umklapp scattering rates comparable to those calculated from first-principles in Si and GaAs [5, 6].

We create large supercells containing millions or tens of millions of atoms with correlated mass disorder configurations. Five atomic species with masses $0.4m_0$, $0.7m_0$, m_0, $1.3m_0$ and $1.6m_0$ are distributed in the supercell with roughly equal concentrations. To produce the disorder configurations, we use a procedure close to that described in Ref [7]. We first generate an auxiliary continuous scalar field $V(\boldsymbol{r})$ with the property that $\frac{1}{N}\sum_{\boldsymbol{r'}} V(\boldsymbol{r'}+\boldsymbol{r})V(\boldsymbol{r'}) = C_{\text{target}}(\boldsymbol{r})$ where $C_{\text{target}}(\boldsymbol{r})$ is the desired correlation function. Since the boundary conditions are periodic making the disorder-averaged field homogeneous, this ensures that $\langle V(\boldsymbol{r})\,V(\boldsymbol{0})\rangle = C_{\text{target}}(\boldsymbol{r})$. We then exploit the fact that the modulus square of the Fourier transform (FT) of the field is the FT of the correlation function. We thus compute the FT $\tilde{C}_{\text{target}}(\boldsymbol{q})$ of $C_{\text{target}}(\boldsymbol{r})$ by a fast Fourier transform (FFT) algorithm, then set the FT of the field as

$$\tilde{V}(\boldsymbol{q}) = \sqrt{\tilde{C}_{\text{target}}(\boldsymbol{q})}\, e^{i\varphi(\boldsymbol{q})} \tag{2}$$

where $\varphi(\boldsymbol{q})$ are random phases that determine different configurations with the same target correlation function. Finally, we use a reverse FFT algorithm to compute $V(\boldsymbol{r})$ and we discretize the field into five different values $\delta m_{\boldsymbol{r}}$ = -0.6, -0.3, 0.0, 0.3 and 0.6. This generates a discrete mass distribution $\delta m_{\boldsymbol{r}}$ whose correlation function $C(\boldsymbol{r})$ is close to the desired correlation function $C_{\text{target}}(\boldsymbol{r})$. Note that this choice of 5 different species is strictly for convenience, any type of alloy can be considered.

2 Perturbative transport scattering rates

We start with the standard lowest-order perturbation formula for scattering of phonon mode $\boldsymbol{k}$ by mass disorder [8, 9], corrected with a factor $1-\cos(\theta_{\boldsymbol{k}+\boldsymbol{q},\boldsymbol{k}})$ to account for the effectiveness of backward vs forward scattering, $\theta_{\boldsymbol{k}+\boldsymbol{q},\boldsymbol{k}}$ being the angle between the velocities of modes $\boldsymbol{k}$ and $\boldsymbol{k}+\boldsymbol{q}$ (see e.g. chapter 16 of [10] or section 8.1.2 of [11]):

$$1/\tau_{\boldsymbol{k}}^{\mathrm{tr}} = \frac{\pi}{\omega_{\boldsymbol{k}}} \sum_{\boldsymbol{q}} \left\langle |g_{\boldsymbol{q}}|^2 \right\rangle (1-\cos(\theta_{\boldsymbol{k}+\boldsymbol{q},\boldsymbol{k}}))\delta(\omega_{\boldsymbol{k}+\boldsymbol{q}}^2 - \omega_{\boldsymbol{k}}^2). \tag{3}$$

$g_{\boldsymbol{q}}$ is the coupling matrix element between mode $\boldsymbol{k}$ and $\boldsymbol{k}+\boldsymbol{q}$, whose disorder-averaged modulus square is given by the Fourier transform of the mass perturbation correlation function $C(\boldsymbol{r}) = \langle \delta m_{\boldsymbol{r}}\, \delta m_{\boldsymbol{0}} \rangle$:

$$\left\langle |g_{\boldsymbol{q}}|^2 \right\rangle = \omega^4 \frac{1}{N} \sum_{\boldsymbol{r}} C(\boldsymbol{r}) e^{-i\boldsymbol{q}\cdot\boldsymbol{r}}. \tag{4}$$

We will now show that correlation functions with power-law long-range decay have a Fourier transform that behaves as a power-law for small wavevectors, irrespective of the precise short-range behavior. Consider an isotropic correlation function that decreases like a power-law beyond a certain cutoff radius r_c: $C(\boldsymbol{r}) = f(||\boldsymbol{r}||)$ with $f(r) = \frac{B}{r^\alpha} e^{-r/\xi}$ for $r > r_c$, where a correlation length ξ has been introduced for regularization purposes and the limit $\xi \to \infty$ will be taken at the end. Keeping only the contribution from the first Brillouin Zone since it is the dominant one at long wavelengths, the average coupling matrix element is given by

$$\left\langle |g_{\boldsymbol{q}}|^2 \right\rangle = \frac{\omega^4}{(2\pi a)^3} \int_{\mathbb{R}^3} d^3\boldsymbol{r}\, f(||\boldsymbol{r}||)\, e^{-i\boldsymbol{q}\cdot\boldsymbol{r}} \tag{5}$$

$$= \frac{\omega^4}{2\pi^2 a^3 q} \int_0^\infty dr\, r f(r) \sin(qr) \tag{6}$$

$$= \frac{\omega^4}{2\pi^2 a^3 q} \int_0^{r_c} dr\, r f(r) \sin(qr) + \frac{\omega^4}{2\pi^2 a^3 q} \int_{r_c}^\infty dr \frac{B}{r^{\alpha-1}} e^{-r/\xi} \sin(qr). \tag{7}$$

Since $f(0) = \langle \delta m^2 \rangle$ is finite, the first term, short-ranged, is bounded as $q \to 0$. As we will see, the other term diverges if $\alpha < 3$. Therefore, we will ignore the first term and focus on the long-ranged term. Introducing the rescaling $u = qr$ yields

$$\left\langle |g_{\boldsymbol{q}}|^2 \right\rangle = \frac{B\omega^4}{2\pi^2 a^3 q^{3-\alpha}} \int_{qr_c}^\infty du \frac{\sin(u)}{u^{\alpha-1}} e^{-u/q\xi}. \tag{8}$$

For $\alpha \geq 1$, the integral converges straightforwardly when $\xi \to \infty$ and $\left\langle |g_{\boldsymbol{q}}|^2 \right\rangle$ behaves as $1/q^{3-\alpha}$ for small q. For $0 < \alpha < 1$, it is helpful to express the sine as a sum of two complex exponentials and then perform an integration by parts:

$$\left\langle |g_{\boldsymbol{q}}|^2 \right\rangle = \frac{B\omega^4}{2\pi^2 a^3 q^{3-\alpha} 2i} \left(\int_{qr_c}^\infty du\, u^{1-\alpha} e^{(i-1/q\xi)u} - \int_{qr_c}^\infty du\, u^{1-\alpha} e^{(-i-1/q\xi)u} \right) \tag{9}$$

$$= \frac{B\omega^4}{2\pi^2 a^3 q^{3-\alpha} 2i} \Bigg(- \frac{(qr_c)^{1-\alpha} e^{(i-1/q\xi)qr_c}}{i - \frac{1}{q\xi}} - \frac{1-\alpha}{i-\frac{1}{q\xi}} \int_{qr_c}^\infty du\, \frac{e^{(i-1/q\xi)u}}{u^\alpha} \tag{10}$$

$$+ \frac{(qr_c)^{1-\alpha} e^{(-i-1/q\xi)qr_c}}{-i - \frac{1}{q\xi}} + \frac{1-\alpha}{-i-\frac{1}{q\xi}} \int_{qr_c}^\infty du\, \frac{e^{(-i-1/q\xi)u}}{u^\alpha} \Bigg)$$

$$= \frac{B\omega^4}{2\pi^2 a^3 q^{3-\alpha}} \Bigg((qr_c)^{1-\alpha} e^{-r_c/\xi} \frac{\cos(qr_c) + \frac{1}{q\xi}\sin(qr_c)}{1 + \frac{1}{q^2\xi^2}} \tag{11}$$

$$+ \frac{1-\alpha}{1+\frac{1}{q^2\xi^2}} \int_{qr_c}^\infty du e^{-u/q\xi} \frac{\cos(u) + \frac{1}{q\xi}\sin(u)}{u^\alpha} \Bigg).$$

In the $\xi \to \infty$ limit, the term in parentheses converges to $(qr_c)^{1-\alpha}\cos(qr_c)+(1-\alpha)\int_{qr_c}^{\infty} du\frac{\cos(u)}{u^\alpha}$, which remains bounded for small q. Thus, in this case also $\left\langle |g_{\boldsymbol{q}}|^2 \right\rangle$ behaves as $1/q^{3-\alpha}$ for small q.

We then calculate the long-wavelength transport scattering rate from equation (3), assuming a Debye dispersion $\omega_{\boldsymbol{k}} = c||\boldsymbol{k}||$ which is valid at low q. Due to the delta function imposing $||\boldsymbol{k}|| = ||\boldsymbol{k}+\boldsymbol{q}||$, the correction factor $1-\cos(\theta_{\boldsymbol{k}+\boldsymbol{q},\boldsymbol{k}})$ becomes $q^2/2k^2$ and the transport scattering rate is

$$1/\tau^{\mathrm{tr}}_{\boldsymbol{k}} \propto \frac{1}{\omega_{\boldsymbol{k}}}\int d^3\boldsymbol{q}\frac{\omega^4_{\boldsymbol{k}}}{q^{3-\alpha}}\frac{q^2}{2k^2}\delta(c^2(\boldsymbol{k}+\boldsymbol{q})^2 - c^2\boldsymbol{k}^2) \tag{12}$$

$$\propto k\int d^3\boldsymbol{q}\, q^{\alpha-1}\,\delta(c^2q^2 + 2c^2\boldsymbol{k}\cdot\boldsymbol{q}) \tag{13}$$

$$\propto k\int_0^{q_D} dq\, q^{1+\alpha}\int_0^{\pi} d\theta\sin(\theta)\delta(q^2 + 2kq\cos(\theta)) \tag{14}$$

$$\propto k\int_0^{q_D} dq\, q^{1+\alpha}\int_{-1}^{1} du\delta(q^2 + 2kqu) \tag{15}$$

$$\propto \int_0^{2k} dq\, q^{\alpha} \tag{16}$$

$$\propto k^{1+\alpha}. \tag{17}$$

We thus find that the transport scattering decreases as $\omega^{1+\alpha}$ instead of the usual ω^4. It is interesting to note that, for the usual perturbative expression without the $1-\cos(\theta_{\boldsymbol{k}+\boldsymbol{q},\boldsymbol{k}})$ factor, the integral (16) becomes $\int_0^{2k} q^{\alpha-2}$, which diverges for $\alpha \leq 1$. It is then necessary to perform a self-consistent Born approximation as in e.g. Ref. [12]. Thus, accounting for backscattering through the correction factor is crucial in the presence of correlations, and the single-particle phonon linewidths give only limited information about the thermal transport properties.

3 Phonon spectral function and transport formalism

Our methods based on the phonon Green's function formalism have been detailed elsewhere [13, 14, 15], but for convenience we will give a brief presentation here. The phonon Green's function of a harmonic disordered supercell containing N sites can be defined as

$$\mathbf{G}(\omega) = \frac{1}{(\omega + i\eta)^2 - \mathbf{D}} \tag{18}$$

where $\mathbf{D} = \frac{1}{\sqrt{\mathbf{M}}}\mathbf{\Phi}\frac{1}{\sqrt{\mathbf{M}}}$ is the dynamical matrix. $\mathbf{M}$ is the diagonal matrix of the atomic masses, $\mathbf{\Phi}$ is the matrix of the interatomic force constants and η is a real positive infinitesimal. In the present case, the disorder on the force constants are neglected, thus only $\mathbf{M}$ and $\mathbf{D}$ are disordered. $\mathbf{G}(\omega)$ is the Fourier transform of the correlation function of the mass-renormalized atomic displacement operators [14].

The spectral function for the plane-wave phonon mode with wavevector $\boldsymbol{k}$ can be defined as

$$A(\boldsymbol{k},\omega) = -\frac{2\omega}{\pi}\mathrm{Im}\left\langle E_{\boldsymbol{k}}\right| \sqrt{\frac{\mathbf{M}_0}{\mathbf{M}}}\mathbf{G}(\omega)\sqrt{\frac{\mathbf{M}_0}{\mathbf{M}}}\left|E_{\boldsymbol{k}}\right\rangle \tag{19}$$

where $\left|E_{\boldsymbol{k}}\right\rangle = \frac{1}{\sqrt{N}}\sum_{\boldsymbol{r}} e^{i\boldsymbol{k}\cdot\boldsymbol{r}}\left|\boldsymbol{r}\right\rangle$ and $\mathbf{M}_0$ is the VCA (disorder-averaged) mass matrix. We remind the reader that the bra-ket notation is used here strictly for convenience, as the vectors denote atomic degrees of freedom and not actual quantum states of the phonon Fock space. That being said, the Green's function formalism used here is fully quantum mechanical. When $A(\boldsymbol{k},\omega)$

exhibits a well-defined peak as a function of frequency (well-defined phonon quasiparticle), the central frequency corresponds to the disorder-renormalized phonon frequency and the full-width at half maximum (FWHM) corresponds to the disorder-limited inverse lifetime of the mode.

The Green-Kubo formalism provides a quantum linear-response expression for the thermal conductivity that fully incorporates disorder effects, including the important ladder vertex corrections associated with the backscattering $1-\cos(\theta)$ factor [11], and does not rely on well-defined phonon quasiparticles:

$$\boldsymbol{\kappa} = \int_0^\infty d\omega\, W_{\mathrm{ph}}(\omega) \frac{\pi k_B^2 T}{3\hbar\Omega} \mathrm{Tr}\left[\mathrm{Im}\mathbf{G}(\omega + \frac{i}{2\tau^{\mathrm{U}}(\omega)})\mathbf{S}\ \mathrm{Im}\mathbf{G}(\omega + \frac{i}{2\tau^{\mathrm{U}}(\omega)})\mathbf{S}\right] \tag{20}$$

where T is the temperature, Ω is the supercell volume, $\boldsymbol{S}_{\boldsymbol{r},\boldsymbol{r'}} = \frac{1}{i}(\boldsymbol{r}-\boldsymbol{r'})D_{\boldsymbol{r},\boldsymbol{r'}}$ is the Hardy heat current operator [16] and $W_{\mathrm{ph}} = \frac{3}{\pi^2}\left(\frac{\hbar\omega}{k_B T}\right)^2\left(-\frac{\partial f_B}{\partial\omega}\right)$ acts as a normalized half-window of width $\approx 2k_BT$ centered on $\omega = 0$, with f_B the Bose-Einstein distribution. The Umklapp phonon-phonon interactions are taken into account as the frequency-dependent inverse lifetime $\frac{1}{\tau^{\mathrm{U}}(\omega)}$ playing the role of an inelastic damping in the phonon Green's function. This approach is broadly equivalent to that recently used for amorphous solids by Isaeva [17], except that we evaluate expression (20) using the CPGF method (see section 4) instead of diagonalizing the dynamical matrix, which allows us to reach very large system sizes up to tens of millions of sites.

We also compute the thermal conductivity along direction x using the standard kinetic expression

$$\kappa = \frac{1}{\Omega}\sum_{\boldsymbol{k}} c_v(\omega_{\boldsymbol{k}}) v_{x,\boldsymbol{k}}^2 \tau_{\boldsymbol{k}}^{\mathrm{tr,tot}} \tag{21}$$

where $c_v(\omega) = \hbar\omega\frac{\partial f_B}{\partial T}(\omega)$ is the heat capacity of phonon modes with frequency ω, $v_{x,\boldsymbol{k}}$ is the velocity of mode $\boldsymbol{k}$ along x. $\tau_{\boldsymbol{k}}^{\mathrm{tr,tot}}$ is the total transport lifetime of mode $\boldsymbol{k}$, given by Matthiessen's rule:

$$\frac{1}{\tau_{\boldsymbol{k}}^{\mathrm{tr,tot}}} = \frac{1}{\tau_{\boldsymbol{k}}^{\mathrm{tr}}} + \frac{1}{\tau^{\mathrm{U}}(\omega_{\boldsymbol{k}})} \tag{22}$$

with $\tau_{\boldsymbol{k}}^{\mathrm{tr}}$ the phonon-disorder transport scattering rate defined in section 2 and $1/\tau^{\mathrm{U}}$ the phonon-phonon Umklapp scattering rate defined in section 1.

At low frequencies, the Green-Kubo conductivity calculations become very costly (see next section) but give the same contribution to κ as the standard kinetic expression using the transport lifetime, because the phonon quasiparticle picture is essentially valid at these low frequencies. Thus, we use the full Green-Kubo method only above 10 rad THz, and we complement it with the simpler kinetic expression below 10 rad THz. Therefore, the dots in Fig. 4 of the main text are obtained strictly speaking from a mix of Green-Kubo CPGF and kinetic theory calculations. The dashed curve, however, are entirely obtained from kinetic theory at all frequencies.

4 The Chebyshev polynomial Green's function method

The Chebyshev polynomials Green's function (CPGF) method has been reviewed in Refs. [18, 19] for electrons, and has been adapted in Refs. [15, 14, 13] for phonons. The central idea is to efficiently evaluate equations (19) and (20) by expanding the phonon Green's function on the Chebyshev polynomial basis:

$$\mathbf{G}(\bar{\omega}) = \sum_{n=0}^{\infty} g_n((\bar{\omega}+i\bar{\eta})^2) T_n(\bar{\mathbf{D}}) \tag{23}$$

where the bar indicates that the spectrum has been rescaled to $[-1,1]$, the $g_n(z)$ are known complex functions:

$$g_n(z) = -i(2-\delta_{n,0})\frac{(z-i\sqrt{1-z^2})^n}{\sqrt{1-z^2}} \tag{24}$$

and the $T_n(\bar{\mathbf{D}})$ are Chebyshev polynomials evaluated for the dynamical matrix, that follow the recursion relation $T_{n+1}(\bar{\mathbf{D}}) = 2\bar{\mathbf{D}}T_n(\bar{\mathbf{D}}) - T_{n-1}(\bar{\mathbf{D}})$ with $T_1(\bar{\mathbf{D}}) = \bar{\mathbf{D}}$ and $T_0(\bar{\mathbf{D}}) = 1$. Equality (23) comes from the identity

$$e^{-izt} = \sum_{n=0}^{\infty} \frac{2i^{-n}}{1+\delta_{n,0}} J_n(t) T_n(z) \tag{25}$$

for $|z| < 1$ with $J_n(t)$ the Bessel function of order n (see equations (5) through (9) in the supplementary material of Ref. [18]).

Since the spectral function for the Bloch mode $\boldsymbol{k}$ is given by eq. (19), the quantities to be calculated are the so-called moments $\mu_{n,\boldsymbol{k}}$:

$$\mu_{n,\boldsymbol{k}} = \langle E_{\boldsymbol{k}}| \sqrt{\frac{\mathbf{M}_0}{\mathbf{M}}} T_n(\bar{\mathbf{D}}) \sqrt{\frac{\mathbf{M}_0}{\mathbf{M}}} |E_{\boldsymbol{k}}\rangle \,, \tag{26}$$

which are computed using the recursion relation between the $T_n(\bar{\mathbf{D}})$. Once this is done, the spectral function can be obtained at any ω at virtually no computational cost. The number of moments necessary for the sum (23) to converge is roughly equal to $1/2\bar{\omega}\bar{\eta}$. Because $\bar{\eta}$ is an artifical broadening and should be smaller than the disorder-induced spectral linewidth, probing modes closer and closer to Γ requires more and more polynomials to be included. To extract the phonon lifetimes of low-frequency modes, we calculate up to 10^6 moments on supercells $305 \times 305 \times 305$. For such system sizes, only one disorder configuration is necessary except when very long-range $1/\sqrt{r}$ are present, in which case we use 4 different configurations to ensure a proper disorder average.

The trace in equation 20 can be called the phonon transport distribution function (TDF) $\Sigma_{\mathrm{ph}}(\omega)$. To calculate it, we use the one-shot stochastic procedure described in Ref. [13, 18]:

$$\Sigma_{\mathrm{ph}}(\omega) = \frac{\pi k_B^2 T}{3\hbar\Omega} \frac{1}{N_r} \sum_{\lambda} \langle \varphi_-^\lambda | \varphi_+^\lambda \rangle \tag{27}$$

with $|\varphi_+^\lambda\rangle = \mathrm{Im}\mathbf{G}(\omega + \frac{i}{2\tau^{\mathrm{U}}(\omega)})\mathbf{S}\,|\lambda\rangle$ and $|\varphi_-^\lambda\rangle = \mathbf{S}\,\mathrm{Im}\mathbf{G}(\omega + \frac{i}{2\tau^{\mathrm{U}}(\omega)})\,|\lambda\rangle$. N_r random vectors $|\lambda\rangle = \sum_{\boldsymbol{r}} e^{i\varphi_{\boldsymbol{r}}}\,|\boldsymbol{r}\rangle$ are defined, with $\varphi_{\boldsymbol{r}}$ a random phase uniformly distributed in the interval $[0, 2\pi]$. The vectors $|\varphi_+^\lambda\rangle$ and $|\varphi_-^\lambda\rangle$ are calculated iteratively for every frequency above 10 rad THz and every temperature. At low frequencies, the Umklapp scattering rates become smaller and smaller, leading to an ever increasing number of terms to be calculated for the Chebyshev series (23) to converge. This is why we rely instead on the simpler kinetic formula below 10 rad THz. Above 10 rad THz, we calculate up to 120000 terms in the series (23) on supercells of size $1200 \times 200 \times 200$. The larger size along the transport direction x allows us to reach the thermodynamic limit by avoiding ballistic effects. We use two disorder configurations for $1/\sqrt{r}$ and $1/r$ correlations, and one configuration for $1/r^2$ correlations and the uncorrelated case.

5 Acoustic phonon spectral functions

We show here in Fig. S1 the phonon spectral function of selected acoustic modes from Fig 3 of the main text in the relevant frequency range (0 to 35 rad THz). They have been calculated from the CPGF method, and the spectral peak broadenings are representative of the disorder-induced lifetime of each mode. Extracting the FWHM of low-frequency modes is computationally difficult for two main reasons:

- The number of terms (moments) that must be included in the Chebyshev expansion (23) of the Green's function is proportional to $\frac{1}{\omega\eta}$, with ω the mode angular frequency and η an artificial broadening that must be much smaller than the mode FWHM. Because the linewidth is proportional to ω^2 for $1/r$ correlations and to ω^4 for the uncorrelated case, the number of moments that must be calculated grows as $1/\omega^3$ for $1/r$ correlations and as $1/\omega^5$ for the uncorrelated case.

- Finite-size effects (i.e. the separation between discrete levels of the disordered system) must be small compared to the mode FWHM, implying that the supercell size must grow as $1/\omega^2$ and $1/\omega^4$ for $1/r$ correlations and no correlations respectively. Computational time is linear with the system size in the CPGF method, but so is memory space. Also, it should be kept in mind that the cubic symmetry in the clean system considered leads to a 48-fold degeneracy for most $\boldsymbol{k}$-points, which increases the level separation substantially. Strictly speaking, these degeneracies are lifted by disorder but this is a small effect at low frequencies.

Of note, the CPGF algorithm relies on an iterative procedure whose parallelization overheads quickly limits the gain obtained from using multiple CPUs. In addition, we have been quite strict when it comes to convergence and have shown only those data points for which we could ascertain that finite size effects are small enough and the number of moments high enough to make the results reliable. From these considerations, we encounter a computational wall at low frequencies. To give an example, the lowest-frequency point shown in Fig. 3 for the uncorrelated case (around 10 rad THz), has been calculated on a $305 \times 305 \times 305$ supercell with 10^6 moments. The calculation for this mode alone took two weeks and around 150GB of RAM. To go lower in frequency would have required both more moments and a larger system, leading to steep costs in both time and memory. For systems featuring spatial correlations, we are more limited by finite-size effects than by the number of moments. Fortunately, the power-law trends are already quite clear in Fig. 3 of the main text, making it unnecessary to go to lower frequencies. We also want to emphasize that the FWHM of the lowest frequency modes shown in Fig. 3 are completely unreachable through exact diagonalization, given the system sizes of several tens of millions of atoms required to calculate them reliably.

6 Numerical evaluation of the thermal conductivity

We show in Fig S2 the same data as in Fig. 4 of the main text in logarithmic scale to emphasize the differences in the values of κ predicted for the various correlation power-laws. In this figure, it is also apparent that perturbative estimates of κ are slightly underestimated compared to CPGF estimates. This is partly due to the fact that the perturbative expression used here does not include the phonon diffusive channel [20]. As mentioned in section 2, if the vertex correction factor $1-\cos(\theta_{\boldsymbol{k}+\boldsymbol{q},\boldsymbol{k}})$ is omitted for correlations decaying slower than $1/r$, the second-order perturbative scattering rates diverge. Numerically, this leads to a non-convergence of the scattering rates as the number of $\boldsymbol{k}$-points increases and the broadening η of the delta peaks in eq (3) decreases. For a given broadening parameter, the scattering rate calculated in this way is also higher than the transport scattering rate (which includes the vertex correction factor) by order of magnitudes. Thus, omitting the vertex correction factor in the perturbative evaluation of κ would lead to a gross overestimation: in the case of $1/\sqrt{r}$ correlations, for instance, the value obtained for the room-temperature thermal conductivity would be $0.075\,\mathrm{W\,m^{-1}\,K^{-1}}$ instead of $2.63\,\mathrm{W\,m^{-1}\,K^{-1}}$. It is clear that vertex corrections are absolutely crucial to capturing the physics of thermal transport in the presence of spatial correlations.

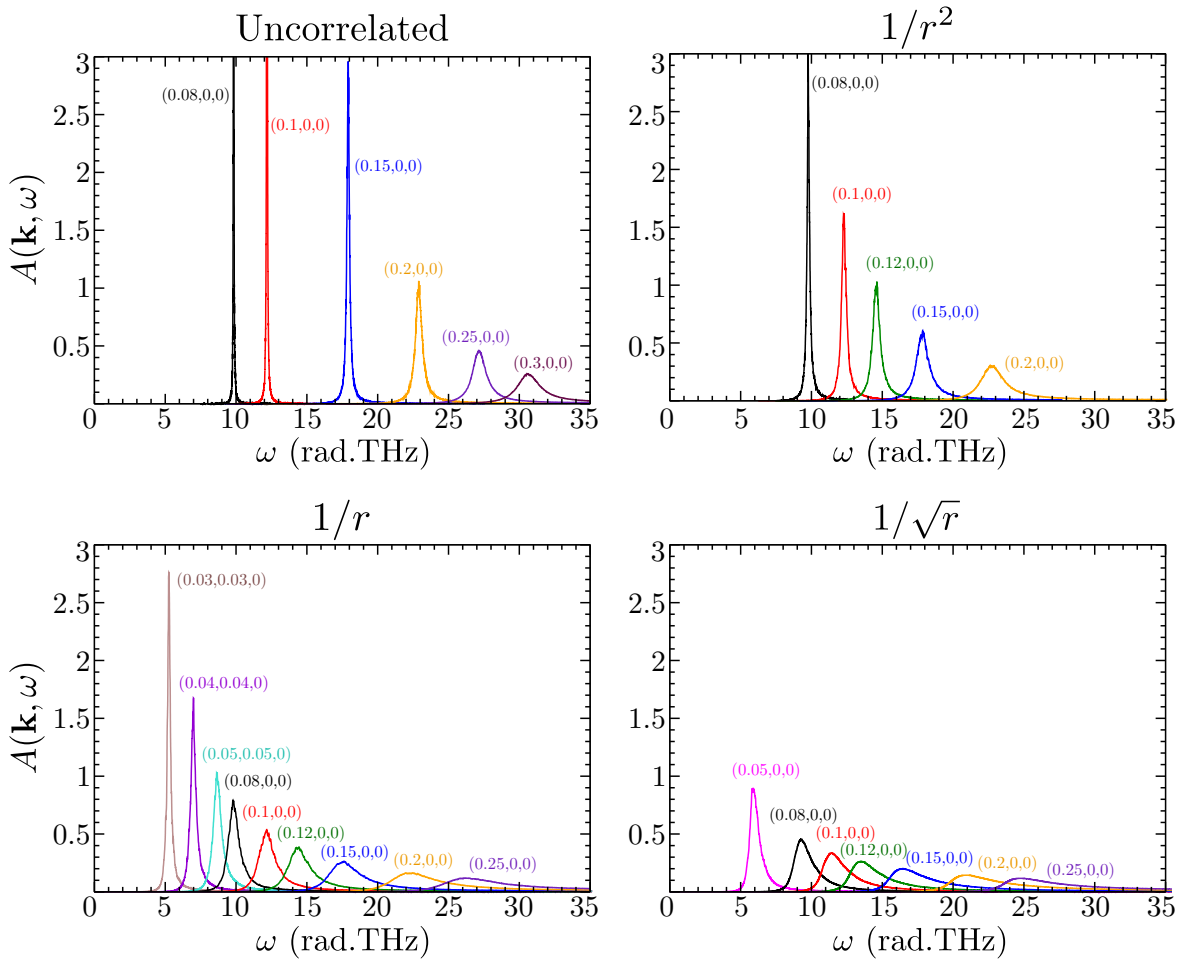

Figure S1: Phonon-spectral function of acoustic modes for several power-law decaying correlations $C(\boldsymbol{r}) \propto 1/r^{\alpha}$ with $\alpha = \infty$ (uncorrelated) and $\alpha = 2$, 1, and 0.5. The curve labels (k_x, k_y, k_z) are the mode wavevectors in units of $2\pi/a$.

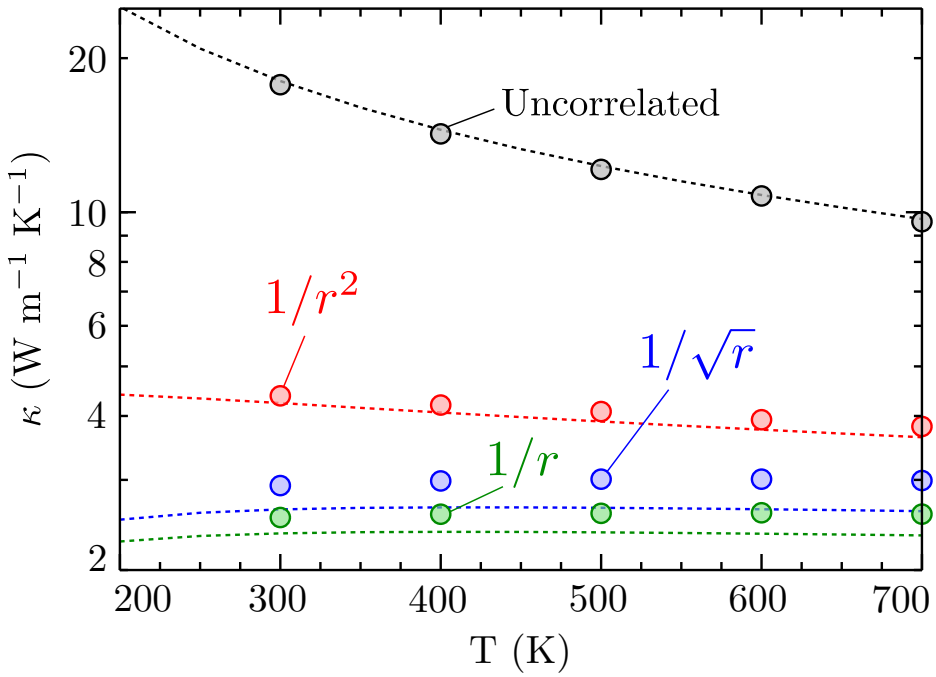

Figure S2: The thermal conductivities for several power-law decaying correlations evaluated through Green-Kubo CPGF calculations above 10 rad THz, with second-order perturbation theory below 10 rad THz (dots) and through perturbation theory only (dashed lines).

7 Optimal correlations to minimize κ

To find the optimal correlation that minimizes the thermal conductivity, we make the fundamental assumption that the simple kinetic expressions (21) and (22) (including the $1-cos(\theta)$ vertex correction factor in the disorder scattering rates) are valid. This assumption is supported by our numerical results (Fig. 4 of the main text). κ then depends on the mass correlations through the phonon-disorder transport scattering rate (see equations (3) and (4)):

$$1/\tau_{\boldsymbol{k}}^{\mathrm{tr}} = \pi\omega_{\boldsymbol{k}}^3 \int \frac{d^3\boldsymbol{q}\,\Omega}{(2\pi)^3}\,\tilde{C}(\boldsymbol{q})(1-\cos(\theta_{\boldsymbol{k}+\boldsymbol{q},\boldsymbol{k}}))\delta(\omega_{\boldsymbol{k}+\boldsymbol{q}}^2-\omega_{\boldsymbol{k}}^2), \tag{28}$$

where $\tilde{C}(\boldsymbol{q}) = \frac{1}{N}\sum_{\boldsymbol{r}} C(\boldsymbol{r})e^{-i\boldsymbol{q}\cdot\boldsymbol{r}}$ is the FT of the correlation function. We then minimize the thermal conductivity as a functional of $\tilde{C}(\boldsymbol{q})$ while keeping the disorder strength $C(\boldsymbol{0}) = \int \frac{d^3\boldsymbol{q}\Omega}{(2\pi)^3}\tilde{C}(\boldsymbol{q})$ constant. This constraint eliminates the obvious solution of introducing more and more disorder, instead answering the question: given a certain amount of defects or disorder, how best to organize it spatially to impede the flow of heat?

Introducing a Lagrange multiplier λ, we are to solve

$$\frac{\delta}{\delta\tilde{C}(\boldsymbol{q})}\left[\int \frac{d^3\boldsymbol{k}}{(2\pi)^3} c_v(\omega_{\boldsymbol{k}}) v_{x,\boldsymbol{k}}^2 \tau_{\boldsymbol{k}}^{\mathrm{tr,tot}} - \lambda \int \frac{d^3\boldsymbol{k}\,\Omega}{(2\pi)^3}\,\tilde{C}(\boldsymbol{k})\right] = 0. \tag{29}$$

Since

$$\frac{\delta\tau_{\boldsymbol{k}}^{\mathrm{tr,tot}}}{\delta\tilde{C}(\boldsymbol{q})} = -(\tau_{\boldsymbol{k}}^{\mathrm{tr,tot}})^2\pi\omega_{\boldsymbol{k}}^3\frac{\Omega}{(2\pi)^3}(1-\cos(\theta_{\boldsymbol{k}+\boldsymbol{q},\boldsymbol{k}}))\delta(\omega_{\boldsymbol{k}+\boldsymbol{q}}^2-\omega_{\boldsymbol{k}}^2), \tag{30}$$

we obtain

$$\pi\int \frac{d^3\boldsymbol{k}}{(2\pi)^3} c_v(\omega_{\boldsymbol{k}}) v_{x,\boldsymbol{k}}^2 \omega_{\boldsymbol{k}}^3 (\tau_{\boldsymbol{k}}^{\mathrm{tr,tot}})^2 (1-\cos(\theta_{\boldsymbol{k}+\boldsymbol{q},\boldsymbol{k}}))\delta(\omega_{\boldsymbol{k}+\boldsymbol{q}}^2-\omega_{\boldsymbol{k}}^2) = -\lambda. \tag{31}$$

To make more analytical progress, we now assume a Debye dispersion $\omega_{\boldsymbol{k}} = c||\boldsymbol{k}||$. Due to isotropy, the left-hand side f_x of equation (31) does not depend on the transport direction considered: $f_x = f_y = f_z = (f_x + f_y + f_z)/3$. Thus:

$$\frac{\pi}{3}\int \frac{d^3\boldsymbol{k}}{(2\pi)^3} c_v(\omega_{\boldsymbol{k}}) c^5 ||\boldsymbol{k}||^3 (\tau_{\boldsymbol{k}}^{\mathrm{tr,tot}})^2 \frac{||\boldsymbol{q}||^2}{2||\boldsymbol{k}||^2} \delta(c^2(\boldsymbol{k}+\boldsymbol{q})^2 - c^2\boldsymbol{k}^2) = -\lambda. \tag{32}$$

Introducing spherical coordinate with θ the angle between $\boldsymbol{k}$ and $\boldsymbol{q}$:

$$\frac{c^3 q^2}{24\pi}\int_0^{k_D} dk\, c_v(\omega_k) k^3 (\tau_k^{\mathrm{tr,tot}})^2 \int_0^{\pi} d\theta \sin(\theta)\, \delta(2kq\cos(\theta) + q^2) = -\lambda, \tag{33}$$

where k_D is the Debye wavevector. The angular integral of the delta function simplifies to $\Theta(2k-q)/(2kq)$ with Θ the Heaviside function, so we have:

$$\frac{c^3 q}{48\pi}\int_{q/2}^{k_D} dk\, c_v(\omega_k) k^2 (\tau_k^{\mathrm{tr,tot}})^2 = -\lambda. \tag{34}$$

Moving the prefactor to the right-hand side and taking the derivative on both sides with respect to q then yields:

$$-\frac{1}{2} c_v(\omega_{q/2})(q/2)^2 (\tau_{q/2}^{\mathrm{tr,tot}})^2 = \frac{48\pi\lambda}{c^3 q^2}. \tag{35}$$

Finally, substituting $q/2 \to q$ we obtain

$$\frac{1}{\tau_q^{\mathrm{tr,tot}}} = \sqrt{\frac{c^3 c_v(\omega_q)}{24\pi|\lambda|}} q^2, \tag{36}$$

as asserted in the main text.

8 Finite correlation length

In order to evaluate the impact of a finite correlation length that would make the correlations short-ranged, we calculate the phonon-disorder transport scattering rates and the thermal conductivities for a correlation function of the form $C(\boldsymbol{r}) \propto \frac{1}{r} e^{-r/\xi}$. Such an r dependence arises naturally in the context of an Ising system, for instance. We make use of the Fermi golden rule to calculate the transport scattering rates (equation (3) and (4)), and we evaluate the thermal conductivity through kinetic theory (equation (21) and (22)). Fig. 4 of the main text shows this methodology to be in excellent agreement with a full Green-Kubo treatment of the thermal conductivity.

We show in Fig S1 the phonon-disorder transport scattering rates for $\xi = 0$ (reference case without correlation), $\xi = 2.47\,\text{Å}$, $4.94\,\text{Å}$, $12.35\,\text{Å}$, $24.70\,\text{Å}$, $49.40\,\text{Å}$ (1, 2, 5, 10, 20 lattice constants respectively) and $\xi = \infty$ corresponding to optimal $1/r$ correlations. For finite correlation lengths, the low-frequency scattering rates always follow an ω^4 Rayleigh law as the phonon wavelength is much greater than the typical cluster length. At intermediate frequencies, there is a crossover towards an ω^2 as the wavelength becomes comparable to the cluster size. However, even for very small correlation lengths down to a few Angströms, the scattering rates are substantially increased at low frequencies compared to the uncorrelated case.

The associated thermal conductivities are shown in Fig S4. Even for ξ equal to one lattice constant, κ is halved compared to the uncorrelated case. The optimal $1/r$ thermal conductivity is recovered as soon as ξ equals 5 to 10 lattice constants. Thus, the inevitable presence of a finite correlation range in actual samples does not seem to be a serious obstacle to manipulating κ through disorder correlations.

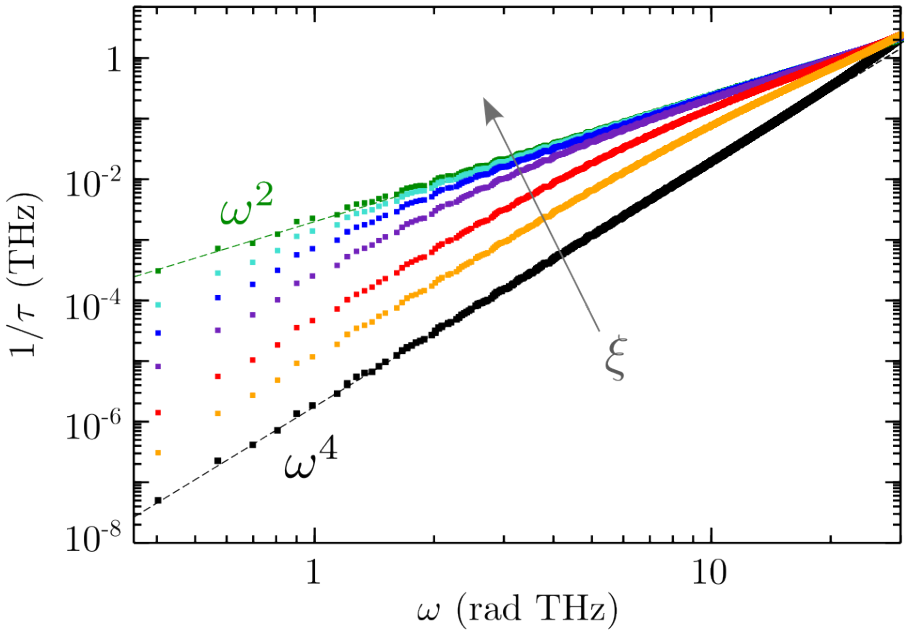

Figure S3: Phonon-disorder transport scattering rates from lowest-order perturbation theory for several values of the correlation length $\xi = 0$ (black, no correlation), a (orange), $2a$ (red), $5a$ (purple), $10a$ (blue), $20a$ (cyan) and $\xi = \infty$ (green).

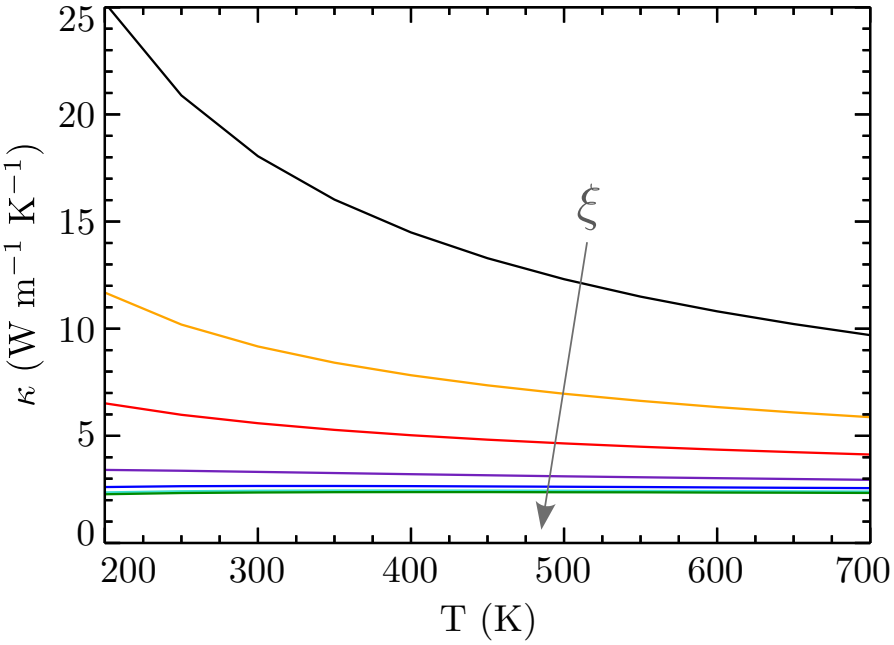

Figure S4: The thermal conductivities evaluated through second-order perturbation theory for several values of the correlation length $\xi = 0$ (black, no correlation), a (orange), $2a$ (red), $5a$ (purple), $10a$ (blue), $20a$ (cyan) and $\xi = \infty$ (green).

References

[1] Changwook Jeong, Supriyo Datta, and Mark Lundstrom. Full dispersion versus Debye model evaluation of lattice thermal conductivity with a Landauer approach. *Journal of Applied Physics*, 109(7):073718, April 2011.

[2] N. Mingo. Calculation of Si nanowire thermal conductivity using complete phonon dispersion relations. *Physical Review B*, 68(11):113308, September 2003.

[3] M. Asen-Palmer, K. Bartkowski, E. Gmelin, M. Cardona, A. P. Zhernov, A. V. Inyushkin, A. Taldenkov, V. I. Ozhogin, K. M. Itoh, and E. E. Haller. Thermal conductivity of germanium crystals with different isotopic compositions. *Physical Review B*, 56(15):9431–9447, October 1997.

[4] Csaba Guthy, Chang-Yong Nam, and John E. Fischer. Unusually low thermal conductivity of gallium nitride nanowires. *Journal of Applied Physics*, 103(6):064319, March 2008.

[5] Tengfei Luo, Jivtesh Garg, Junichiro Shiomi, Keivan Esfarjani, and Gang Chen. Gallium arsenide thermal conductivity and optical phonon relaxation times from first-principles calculations. *EPL (Europhysics Letters)*, 101(1):16001, January 2013.

[6] Jivtesh Garg, Nicola Bonini, Boris Kozinsky, and Nicola Marzari. Role of Disorder and Anharmonicity in the Thermal Conductivity of Silicon-Germanium Alloys: A First-Principles Study. *Physical Review Letters*, 106(4):045901–045901, January 2011.

[7] F. M. Izrailev and N. M. Makarov. Anomalous transport in low-dimensional systems with correlated disorder. *Journal of Physics A: Mathematical and General*, 38(49):10613–10637, November 2005.

[8] Shin-ichiro Tamura. Isotope scattering of dispersive phonons in Ge. *Physical Review B*, 27(2):858–866, January 1983.

[9] Shin-ichiro Tamura. Isotope scattering of large-wave-vector phonons in GaAs and InSb: Deformation-dipole and overlap-shell models. *Physical Review B*, 30(2):849–854, July 1984.

[10] N W Ashcroft and N D Mermin. *Solid State Physics*. Saunders College, 1976.

[11] G D Mahan. *Many Particle Physics, Third Edition*. Plenum, New York, 2000.

[12] Sajeev John and Michael J. Stephen. Wave propagation and localization in a long-range correlated random potential. *Physical Review B*, 28(11):6358–6368, December 1983.

[13] S. Thébaud, T. Berlijn, and L. Lindsay. Perturbation theory and thermal transport in mass-disordered alloys: Insights from Green's function methods. *Physical Review B*, 105(13):134202, April 2022.

[14] S. Thébaud, C. A. Polanco, L. Lindsay, and T. Berlijn. Success and breakdown of the T-matrix approximation for phonon-disorder scattering. *Physical Review B*, 102(9):094206, September 2020.

[15] G. Bouzerar, S. Thébaud, S. Pecorario, and Ch. Adessi. Drastic effects of vacancies on phonon lifetime and thermal conductivity in graphene. *Journal of Physics: Condensed Matter*, 32(29):295702, April 2020.

[16] Robert J Hardy. Energy-Flux Operator for a Lattice. *Physical Review*, 132(1):168–177, October 1963.

[17] Leyla Isaeva, Giuseppe Barbalinardo, Davide Donadio, and Stefano Baroni. Modeling heat transport in crystals and glasses from a unified lattice-dynamical approach. *Nature Communications*, 10:3853, August 2019.

[18] Aires Ferreira and Eduardo R Mucciolo. Critical Delocalization of Chiral Zero Energy Modes in Graphene. *Physical Review Letters*, 115(10):106601–106601, August 2015.

[19] Alexander Weiße, Gerhard Wellein, Andreas Alvermann, and Holger Fehske. The kernel polynomial method. *Reviews of Modern Physics*, 78(1):275–306, March 2006.

[20] Michele Simoncelli, Nicola Marzari, and Francesco Mauri. Unified theory of thermal transport in crystals and glasses. *Nature Physics*, 15(8):809–813, August 2019.